Journal of Power Sources 373 (2018) 150–160

Contents lists available at ScienceDirect

Journal of Power Sources

journal homepage: www.elsevier.com/locate/jpowsour

A combined theoretical-experimental study of interactions between vanadium ions and Nafion membrane in all-vanadium redox flow batteries

Nadia N. Intan[a], Konstantin Klyukin[a], Tawanda J. Zimudzi[b], Michael A. Hickner[b], Vitaly Alexandrov[a,c,*]

[a] Department of Chemical and Biomolecular Engineering, University of Nebraska-Lincoln, Lincoln, NE 68588, USA
[b] Department of Materials Science and Engineering, The Pennsylvania State University, University Park, PA 16802, USA
[c] Nebraska Center for Materials and Nanoscience, University of Nebraska-Lincoln, Lincoln, NE 68588, USA

HIGHLIGHTS

- Nafion tends to have contact pair mechanism interactions with aqueous vanadium cations.
- Strong cation binding to Nafion induces peak splitting observed in IR spectra.
- DFT calculations help explain changes in IR spectra.

GRAPHICAL ABSTRACT

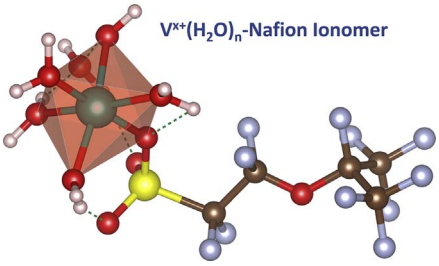

ARTICLE INFO

Keywords:
Nafion
Vanadium redox flow batteries
ab–initio calculations
Infrared spectroscopy*MSC:*
00-01
99-00

ABSTRACT

Vanadium redox flow batteries (VRFBs) are a promising solution for large-scale energy storage, but a number of problems still impede the deployment of long-lifetime VRFBs. One important aspect of efficient operation of VRFBs is understanding interactions between vanadium species and the membrane. Herein, we investigate the interactions between all four vanadium cations and Nafion membrane by a combination of infrared (IR) spectroscopy and density-functional-theory (DFT)-based static and molecular dynamics simulations. It is observed that vanadium species primarily lead to changes in the IR spectrum of Nafion in the SO_3^- spectral region which is attributed to the interaction between vanadium species and the SO_3^- exchange sites. DFT calculations of vanadium−Nafion complexes in the gas phase show that it is thermodynamically favorable for all vanadium cations to bind to SO_3^- via a contact pair mechanism. Car-Parrinello molecular dynamics-based metadynamics simulations of cation-Nafion systems in aqueous solution suggest that V^{2+} and V^{3+} species coordinate spontaneously to SO_3^-, which is not the case for VO^{2+} and VO_2^+. The interaction behavior of the uncycled membrane determined in this study is used to explain the experimentally observed changes in the vibrational spectra, and is discussed in light of previous results on device-cycled membranes.

1. Introduction

Redox flow batteries (RFBs) are currently experiencing rapid growth in interest as attractive candidates for large-scale energy storage applications because they are capable of storing multimegawatt-hours of electrical energy from intermittent renewable sources such as wind and solar [1,2]. RFBs release or store energy when redox-active species dissolved in liquid electrolytes undergo electrochemical reactions at the electrode surfaces [3]. Out of many RFB chemistries that have been developed to date, the all-vanadium RFB (VRFB) has received the most

* Corresponding author. Department of Chemical and Biomolecular Engineering, University of Nebraska-Lincoln, Lincoln, NE 68588, USA.
E-mail addresses: mah49@psu.edu (M.A. Hickner), valexandrov2@unl.edu (V. Alexandrov).

https://doi.org/10.1016/j.jpowsour.2017.10.050
Received 29 June 2017; Received in revised form 16 September 2017; Accepted 16 October 2017
Available online 09 November 2017
0378-7753/

attention [4–11]. Aqueous VRFBs use only one electroactive element (vanadium) for the entire redox cell with the V^{2+}/V^{3+} redox couple in the negative half-cell (anolyte) and the VO^{2+}/VO_2^+ couple in the positive half-cell (catholyte) separated by an ion-exchange membrane to allow the migration of protons or sulfate/bisulfate. The use of the same element in both electrolyte reservoirs results in easier electrolyte regeneration and lower cross-contamination due to the crossover of vanadium ions through the membrane between the two electrolyte compartments. However, during long-term VRFB cell cycling, diffusion of vanadium ions through the membrane and their interaction with membrane constituents result in degradation of membrane components, capacity loss and electrolyte contamination [12]. Therefore, it is critical to understand how aqueous vanadium ions interact with the membranes at the molecular scale to help guide the design of more selective and chemically stable membranes.

The ideal membrane for VRFB applications should possess high selectivity to facilitate facile transport of protons or other supporting electrolyte anions or cations to complete the electrical circuit [13], but the membrane also needs to be impermeable to vanadium cations to prevent self-discharge reactions and capacity decay [14]. Other desired properties of the VRFB membrane include low water uptake, good physical strength, high chemical and thermal stability, and low production cost [15]. The most widely used membranes for RFBs are made of perfluorosulfonic acid (PFSA) polymers. Of particular importance among PFSA membranes is Nafion [16] characterized by its high ionic conductivity and high chemical stability, and it has been extensively used in fuel cells and batteries since its development in 1960s. Nafion is a sulfonated fluorocarbon polymer composed of a hydrophobic fluorocarbon teflon-based backbone with perfluoroether side chains terminated by strongly hydrophilic $-CF_2SO_3H$ acid groups. In the presence of water, protons as well as the sulfonate groups of Nafion are in solvated form which greatly facilitates the hopping mechanism of protons. This hopping mechanism is widely known as the Grotthuss mechanism and is defined as the diffusion of protons through the H-bond network by the formation or cleavage of covalent OH bonds [17].

In practice, not only protons but also significant amounts of water and vanadium ions are transferred across the Nafion membrane during the VRFB operation. In the past, the effect of hydration on ionic conductivity of Nafion has been extensively examined both experimentally and theoretically [18,19]. In the context of VRFBs, despite a series of both experimental and theoretical investigations [20–23], it remains ambiguous whether the contact pairs with covalent-type bonding between vanadium ions and sulfonate sites of Nafion are formed, or if these species interact electrostatically through the solvent molecules thus exhibiting solvent-separated ion pair-type interactions. Several computational studies have recently focused on understanding the interaction mechanisms between vanadium ions and Nafion, but the results were inconclusive [20,22]. It is also still unclear why after VRFB cycling only the VO^{2+} species were experimentally identified inside Nafion membranes [21], while all four vanadium cations are present in the system. Although different types of cation- and anion-exchange membranes have been developed in recent years that are characterized by better ion selectivity and lower costs than Nafion, even the behavior of Nafion as the prototypical PFSA membrane in the presence of vanadium ions at the molecular level is still lacking. Detailed microscopic information about the interaction of Nafion with aqueous vanadium ions versus other metal ions would enable the development of efficient strategies to prevent vanadium crossover and decrease capacity fading of the VRFBs.

In a recent modeling study employing density-functional-theory (DFT) calculations at the B3LYP/6-311G++ level of theory [22] interactions between hydrated vanadium cations and triflic (CF_3SO_3H) acid mimicking the terminal functional group of PFSA membranes were investigated in the gas-phase in conjunction with a continuum solvation model. It was suggested that none of the vanadium cations should covalently bind to the sulfonate group of triflic acid, but rather interact with the SO_3^- site through the hydration shell (solvent share mechanism). It should be noted, however, that although triflic acid does resemble Nafion as both have fluorinated backbone and sulfonic acid head group, the polymer chain of Nafion is different making it a much weaker acid (by about three orders of magnitude) than triflic acid with a pK_a value of about -6 [18,19]. Another recent gas-phase DFT study has focused on the interaction between the aqua-vanadyl ion $VO(H_2O)_5^{2+}$ and the SO_3^- group of Nafion using a small Nafion ionomer model [20]. The authors investigated the energetics of vanadyl binding to SO_3^- through both solvent share and contact pair mechanisms, but the results were not conclusive as to what interaction mechanism should be more favorable.

It should be pointed out that the questions about the interaction mechanisms of Nafion with many other aqueous cations is still largely unresolved despite years of research [23–27]. For instance, it was suggested that Li^+, Na^+ and K^+ should bind covalently to the sulfonate sites of Nafion preserving the 3-fold local symmetry, based on the combination of IR spectroscopy and gas-phase DFT calculations [25,26]. However, these results seem to contradict other DFT-based computational studies of Li^+ interacting with triflate $CF_3SO_3^-$ [28] and Na^+ interacting with SO_3^- of Nafion [19] which show preference for these cations toward monodentate binding. This type of covalent interaction should break the local C_{3v} symmetry of the terminal SO_3^- group which may affect the SO_3^- IR spectral region.

In this paper we present the results of our systematic investigation of the interaction between all four aqueous vanadium cations and the sulfonic acid group of Nafion by means of IR spectroscopy and DFT-based static and molecular dynamics simulations.

2. Experimental details

An approximately 150 μm thick Nafion membrane was prepared by solvent casting from an alcohol dispersion containing 20 wt% Nafion (DE2021, Ion power, New Castle, DE) at 80 °C followed by drying at 65 °C under vacuum for 24 h. The complete removal of solvent was confirmed by the absence of solvent peaks in the infrared spectrum of the membrane. The membrane was subsequently stored under vacuum at room temperature and used to generate vanadium complex samples within 72 h of preparation. To generate vanadium complex samples the 2.5 cm×1 cm sections of the Nafion membrane were soaked in a salt solution containing the vanadium ion of interest for 24−48 h rinsed in de-ionized (DI) water to remove residual ions and dried under vacuum at 30 °C for 24 h before collecting spectra under a constant flow of dry nitrogen. Spectra were collected on a Vertex 70 spectrometer (Bruker, Billerica, MA) equipped with a wide band Mercury-Cadmium-Telluride (MCT) detector. The oxidation states of vanadium were confirmed by the color of the solution, and more precisely by UV–Vis measurements (see Supporting Information for more details). When removed from solution, the membrane acquired the color of the solution, and maintained this color for the next 4−5 days. In the case of V^{2+} oxidation occurred rapidly upon removing the membrane from solution, and therefore the spectra were obtained directly after removing the membrane from solution and after drying overnight.

Measurements were conducted in attenuated total reflection geometry on a horizon ATR accessory (Harrick, Pleasantville, NY) at 45° incident angle with a Ge attenuated total reflection (ATR) crystal. All spectra were collected as an average of 400 scans at 4 cm^{-1} resolution. The resultant spectra were 2 point baseline corrected in the Opus software package (Bruker, Billerica, MA) with no further spectral manipulations performed.

3. Computational details

3.1. Gas-phase calculations

The structure of Nafion used in this study is shown in Fig. 1. For

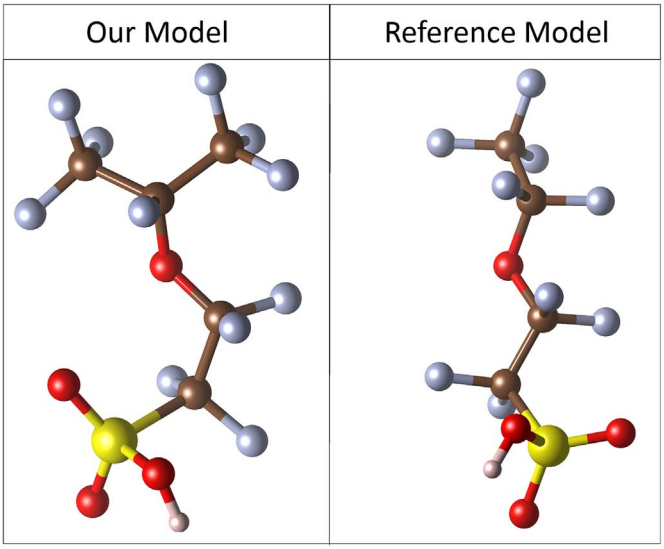

Fig. 1. Atomic structures of the Nafion ionomer used in this study ($((CF_3)_2CFOCF_2CF_2SO_3H$) and in the previous computational work ($CF_3CF_2OCF_2CF_2SO_3H$) [32].
Color representation: blue:fluorine, brown:carbon, yellow:sulfur, red:oxygen, white:-hydrogen. (For interpretation of the references to colour in this figure legend, the reader is referred to the web version of this article.)

each vanadium ion (V^{2+}, V^{3+}, VO^{2+} and VO_2^+) two different mechanisms of interaction with Nafion were considered. The first mechanism corresponds to the case where a vanadium ion forms covalent bonds with the oxygen atoms of sulfonate group of Nafion with a characteristic distance of 2.2 Å, which is termed as the contact pair (CP) mechanism. The second type of interaction is the solvent share (SS) mechanism in which the vanadium cations are indirectly bound to Nafion through hydrogen bonds between water molecules from the first hydration shell of a vanadium ion and the oxygen atoms of the sulfonate group. To obtain the energetics and vibrational spectra of the structures in gas-phase, DFT optimizations of a series of atomic configurations were carried out at zero Kelvin using 6-311G** basis set and the B3LYP [29] hybrid exchange-correlation functional as implemented in the NWChem code [30]. The convergence of both total energy and threshold of the orbital gradient were set to 10^{-10} a.u., while the accuracy for the initial Fock-matrix construction from the atomic guess was set to 10^{-12} a.u. The enthalpies of reactions were calculated at 0 K, while for the calculations of vibrational frequencies the temperature of the systems were raised to room temperature (298.15 K). Some additional calculations were performed using the same basis set and the X3LYP [31] functional.

3.2. Aqueous-phase Car-Parrinello molecular dynamics simulations

The interactions between Nafion and all four vanadium cations in aqueous solution were investigated by employing canonical ensemble Car-Parrinello molecular dynamics (CPMD) [33] approach. Simulations for each vanadium ion with the Nafion ionomer were independently performed using a cubic box of 13 Å length subject to periodic boundary conditions. Each box was filled with 52 H_2O molecules to make the water density of approximately of 1 g/cm^3. Density-functional-theory (DFT) formalism within the plane-wave basis set was employed as implemented in the NWChem code [30]. Exchange and correlation were treated using the Perdew-Burke-Ernzerhof (PBE) [34] functional within the generalized gradient approximation (GGA). Troullier-Martins pseudopotentials [35] were used to describe vanadium and fluorine atoms, while Hamann-type pseudopotentials [36,37] were used for all other atoms. The kinetic energy cutoffs of 100 and 200 Ry were applied to expand the Kohn-Sham electronic wave functions and charge density, respectively. The Nose-Hoover thermostat [38,39] was used to keep simulation temperature at 300 K, while all hydrogen atoms of water molecules were replaced with deuterium. All simulations were performed at constant volume with a fictitious electronic mass of 600 au and a simulation time step of δt = 5 a.u. (0.121 fs). Each system was initially pre-equilibrated with a QM/MM potential for 3.6 ps [40] followed by a subsequent 10.8 ps CPMD equilibration, while the total production time was 5 ps for all aqueous systems.

A CPMD-based metadynamics technique [41,42] was used to compute the free energy profiles for both attachment and detachment of vanadium ions to and from the SO_3^- group of Nafion to obtain insights into the kinetics of these processes in aqueous solution at 300 K. Metadynamics simulations were performed using equilibrated systems from the last block of the CPMD production runs, using the bond distance between vanadium and oxygen of the sulfonate group in Nafion as the collective variable. The height and width of the repulsive Gaussian hills were set to 0.0005 a.u. and 0.07 a.u., respectively, which were added to the potential every 200 δt.

3.3. Vibrational frequency calculations and normal mode analysis

The analysis of DFT computed vibrational frequencies and normal modes were performed using the Chemcraft package [43]. Normal mode animations produced using Chemcraft are also provided in Supporting Information.

4. Results and discussion

4.1. IR spectroscopy

As can be seen from Fig. 2, the experimental spectra obtained for Nafion is in good agreement with previous studies [27,44,45]. The upper limit of IR frequency spectra in this work is 1500 cm^{-1}, as the peaks at higher frequency belong to the stretching of OH bonds in water molecules. In general, the IR spectra of all considered cation−Nafion complexes appear to be similar. The main difference is whether the peak at 950-1000 cm^{-1} is split into a doublet or remains as a singlet. It is observed that this peak is split for all vanadium−Nafion complexes as well as for pure Nafion in acid form, while in the case of Li^+/Na^+−Nafion complexes this peak remains as a singlet. The origin of the peaks in the 950-1000 cm^{-1} region, regardless of whether they appear as a singlet or a doublet, have been the subject of an ongoing debate by both experimentalists and theorists. Several previous studies [46,47] suggested that the peaks in this range are primarily associated with the

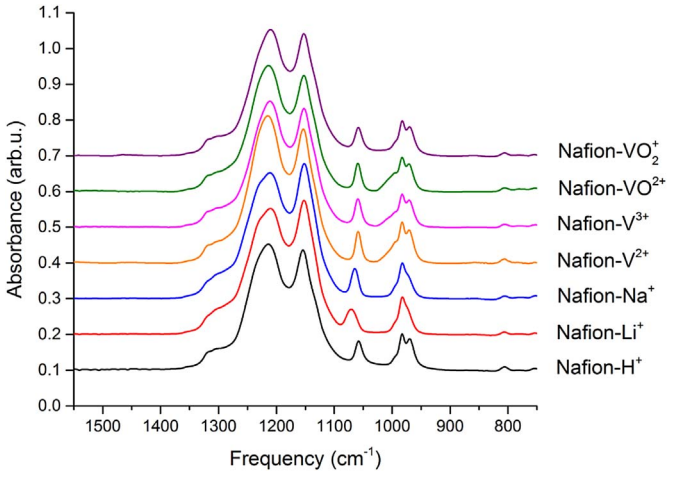

Fig. 2. Experimental infrared (IR) spectra for different cation−Nafion systems.

vibrations of C-O-C ether linkage group in Nafion. In contrast, other works proposed that these peaks are due to the vibrations of SO_3^- group in Nafion [48,49]. The shoulder at 992 cm^{-1} is attributed to the CF_2 deformation that overlaps the 983 cm^{-1} ether peak. The 983 cm^{-1} peak changes with hydration revealing the CF_2 shoulder under certain conditions [27].

4.2. Gas-phase calculations of vanadium−Nafion interaction energetics

We start by performing DFT calculations to probe the energetics of interaction between aqueous vanadium cations and sulfonic group of Nafion ionomer in the gas-phase. The molecular structure of Nafion ionomer used in our study is the same [20] or very similar [32,50] to the molecular models of Nafion employed in previous first-principles investigations and is shown in Fig. 1. The hydration of vanadium ions has been recently examined in both gas-phase DFT [20,51] and aqueous-phase CPMD [10] simulations. It was demonstrated that the first hydration shell of both V^{2+} and V^{3+} contains six water ligands, while VO^{2+} is coordinated to five and VO_2^+ to three water molecules. The starting atomic configurations for gas-phase optimizations of vanadium−Nafion complexes were prepared based on the CPMD results discussed below, as well as using manually constructed structures with different number of V−O bonds between hydrated vanadium ions and SO_3^- group of Nafion.

The formation enthalpies for vanadium−Nafion complexes are computed according to the following generalized reaction:

$$\text{Nafion}^- + V^{z+}(H_2O)_n \rightarrow \text{Nafion} - V^{(z-1)+}(H_2O)_{(n-1)} + H_2O \quad (1)$$

For this reaction we consider molecular structures of the complexes between the bare Nafion ionomer and various aqueous cations for both CP and SS interaction mechanisms. The most energetically favorable atomic configurations of vanadium−Nafion complexes are found to be all monodentate CP and are shown in Fig. 3, while the corresponding energies are listed in Table 1. Additionally, the computed reaction enthalpies for reaction (1) with protonated Nafion (Nafion−H) provided in SI (Table S1) indicate that except VO_2^+ all vanadium species prefer to displace H^+ ion from Nafion.

Some previous studies suggested that the X3LYP functional may provide a more accurate ΔH^f as the description of van der Waals interactions is improved with respect to B3LYP [50]. Therefore, we also carried out calculations of interaction energetics employing the X3LYP functional along with the same basis set for comparison on the example of V^{2+}−Nafion system. The results obtained for reaction (1) with the protonated Nafion indicate that the CP configuration is more stable than SS by about 0.55 eV in X3LYP, in good agreement with 0.66 eV computed using B3LYP.

It is worth noting that our predictions are qualitatively different from those previously made in a computational study of the interaction between hydrated vanadium cations and triflic acid (CF_3SO_3H) by means of gas-phase DFT calculations where the authors reported SS structures as the most stable configurations [22]. As discussed above, however, Nafion is a much weaker acid than triflic acid with a pK_a value of about −6 [18,19], and is therefore expected to have a stronger driving force to form contact ion pairs with vanadium cationic species than triflic acid.

In contrast to vanadium species, CP and SS complexes of both Li^+ and Na^+ appear to exhibit similar energetics of formation with a slight preference for CP configurations (Table 1). The small difference in the enthalpy of formation between the two interaction mechanisms signifies that both Li^+ and Na^+ cations are only weakly bonded to Nafion. This weak bonding is further confirmed by our 10 ps long CPMD simulations in which Li^+ and Na^+ ions in aqueous solution are switching between CP and SS configurations (Fig. 5a). The conversion between CP and SS configurations seen in CPMD simulations in turn will have important implications for explanation of the differences in IR spectra across various cation−Nafion systems observed experimentally.

4.3. Aqueous-phase CPMD simulations

In addition to the gas-phase DFT calculations, we perform detailed CPMD simulations of cation−Nafion systems in aqueous solution at room temperature by using the simulation box setup shown in Fig. 4. To sample different possible binding configurations between aqueous cations and the SO_3^- group of Nafion, a series of starting geometries for both contact pair (CP) and solvent share (SS) interaction mechanisms are considered, similarly to the gas-phase calculations. In the case of CP structures, cations are forced to form various numbers of bonds with oxygen atoms of the SO_3^- head group resulting in mono-, bi- and tridentate covalent bonding configurations. For the SS arrangements the distance between an aqueous cation and the SO_3^- group is set large enough to ensure the interaction through one H_2O of the first hydration shell of a cation rather than through covalent bonding.

CPMD simulations involving CP structures indicate that all four vanadium cations prefer to form one covalent bond with one oxygen atom of SO_3^-, while bi- and tridentate complexes always converge to singly-bonded vanadium−Nafion structures during CPMD simulations, in agreement with our gas-phase calculations. When modeling SS complexes, we also find that aqueous V^{2+} and V^{3+} ions tend to spontaneously form singly-bonded CP structures from initial SS configurations suggesting zero activation barrier of attachment to the SO_3^- head group of Nafion in water at 300 K. Our analysis of the average V−O bond distance for each monodentate vanadium−Nafion complex shows that the bond tends to be longer in aqueous-phase CPMD simulations than those obtained in the gas-phase calculations due to both the different functionals employed (PBE vs. B3LYP, respectively), as well as the effect of hydrogen bond network when using an explicit water environment.

For Li^+ and Na^+ ions we also consider several possible interaction mechanisms with Nafion. In the case of interaction with the SO_3^- group we test mono-, bi-, tridentate, and aggregate structures. In addition to SO_3^-, we examine the F atom next to the SO_3^- group in the backbone and the C−O−C ether linkage in Nafion as plausible sites for the binding of Li^+ and Na^+ ions to Nafion. The last two binding sites are only considered for the monodentate geometry using both CP and SS configurations.

We find that for the SO_3^- binding site, all starting geometries other than monodentate turn out to be unstable. It is observed that Li^+ and Na^+ ions constantly flip between CP and SS configurations throughout the simulation confirming the small difference in the enthalpy of formation obtained in the gas-phase calculations for these two configurations, as demonstrated by the pair distribution function shown in Fig. 5a. For other binding sites, the monodentate CP starting configuration is found to be unstable in all cases. Depending on the position of the water molecules of the cations' first hydration shell, it may turn into SS configuration, where the complex is held by hydrogen bonds between water molecules in the first hydration shell and F atoms of Nafion backbone. From our CPMD runs, the coordination number of Li^+ is found to fluctuate between two and four. For Na^+ the coordination number is determined to be five in the case of SS, but ranges from four to six when Na^+ adopts CP configuration with Nafion (Fig. 5b). Overall, our results are in agreement with previous DFT-based studies demonstrating the favorability of asymmetric monodentate rather than aggregate or tridentate symmetric attachment of Li^+ to triflate anion [28] and of Na^+ to Nafion [19].

We then carried out CPMD-based metadynamics simulations to obtain the free-energy profiles for both attachment and detachment of vanadium ions to and from the sulfonate group of Nafion in aqueous solution at 300 K. To this end, we start from the last timeframe of the CPMD production runs and evaluate the barriers between CP and SS atomic configurations. The estimated barriers for both adsorption and desorption process of all four vanadium species from and onto Nafion

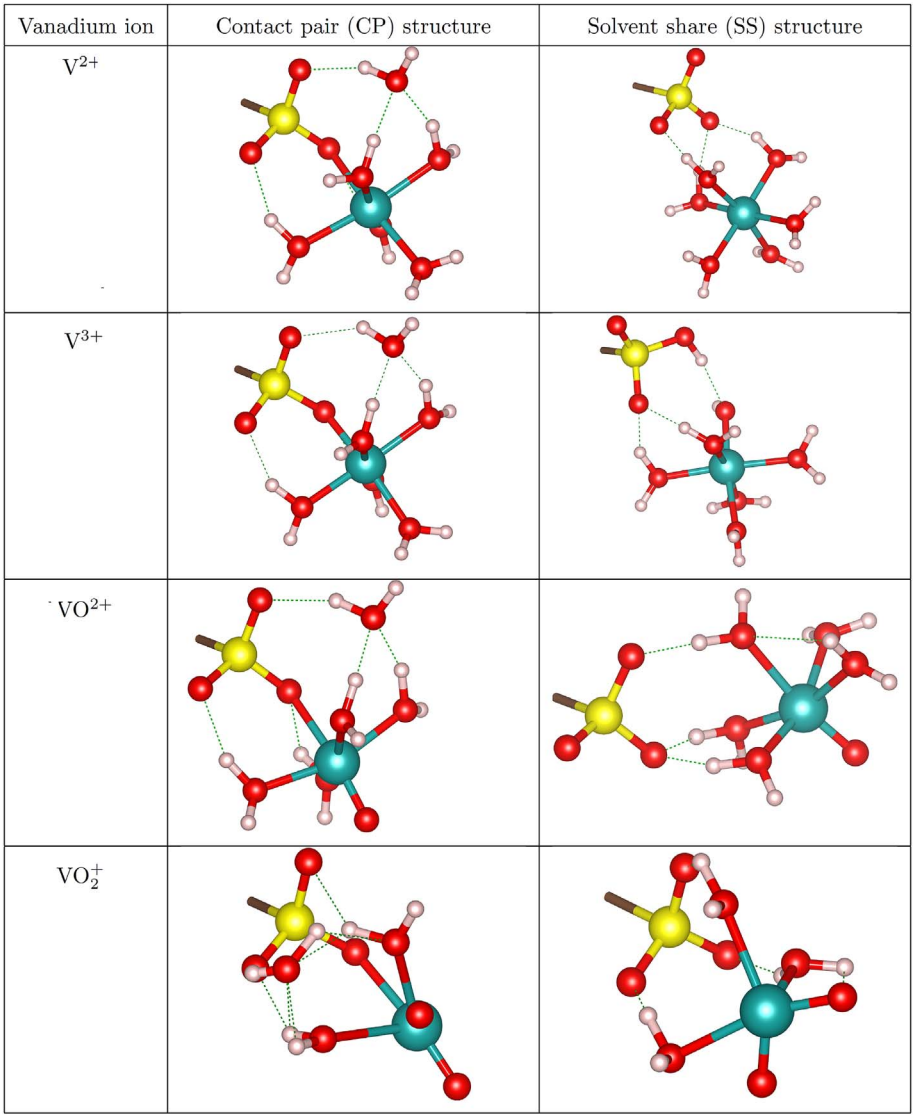

Fig. 3. The most favorable contact pair (CP) and solvent share (SS) atomic configurations between aqueous vanadium ions and the Nafion model ionomer as found in DFT calculations (only the SO_3^- group of Nafion is shown for clarity). The corresponding formation energies are listed in Table 1.
Color representation: yellow: sulfur, red: oxygen, white: hydrogen, green: vanadium. (For interpretation of the references to colour in this figure legend, the reader is referred to the web version of this article.)

Table 1
Enthalpies of formation (in eV) of cation−Nafion complexes for the contact pair (ΔH^f_{CP}) and solvent share (ΔH^f_{SS}) types of binding computed by DFT according to reaction (1).

Cation	ΔH^f_{CP}	ΔH^f_{SS}	ΔH^f_{CP} - ΔH^f_{SS}
V^{2+}	−8.28	−7.62	−0.66
V^{3+}	−13.74	−12.92	−0.82
VO^{2+}	−9.05	−8.30	−0.75
VO_2^+	−5.33	−5.04	−0.30
Li^+	−4.47	−4.42	−0.05
Na^+	−4.29	−4.20	−0.09

are presented in Table 2.

It can be seen from Table 2 that the energy barrier for aqueous vanadium ions to detach from Nafion is the highest for V^{3+}, followed by doubly charged VO^{2+} and V^{2+} and then singly charged VO_2^+, which could be expected based on the electrostatic interaction between the vanadium cations and SO_3^- group. Thus, it is the V^{3+} species that requires the largest amount of energy to break the V−O bond suggesting that V^{3+}−Nafion complex is the most stable out of all vanadium−Nafion complexes in aqueous solution. We also find that the attachment of

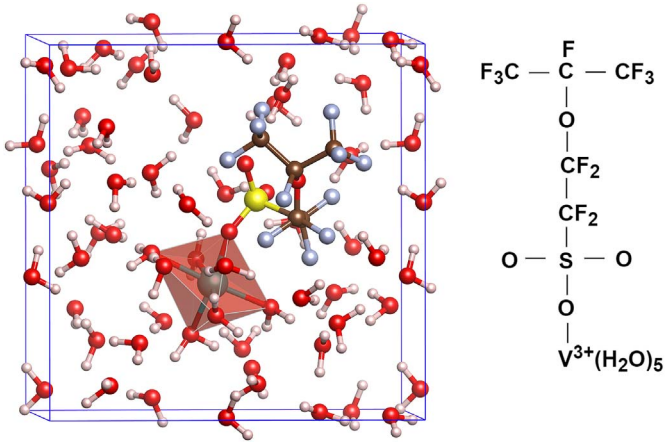

Fig. 4. Simulation box comprised of V^{3+}−Nafion system embedded in water solution used for CPMD calculations.

vanadium ions to the SO_3^- site from the SS to CP configuration is spontaneous for aqueous V^{2+} and V^{3+} ions. In the case of VO_2^+ and VO^{2+} adsorption to SO_3^-, we could only evaluate the lower bound for the

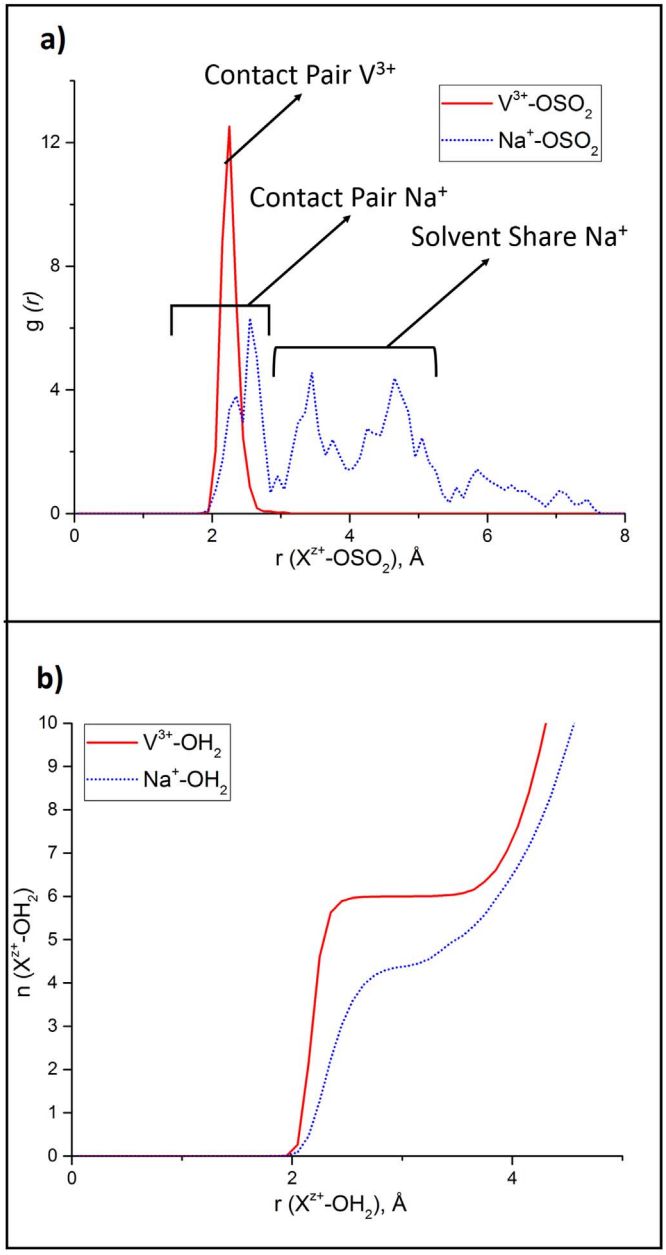

Fig. 5. a) Pair distribution functions g(r) between cations (V^{3+} and Na^{+}) and the oxygen atom of the SO_3^- group of Nafion ionomer obtained from a 10.8 ps CPMD trajectory; b) the corresponding running coordination numbers for cations (V^{3+} and Na^{+}) with water molecules.

Table 2
Estimated free-energy barriers (in eV) based on the free-energy profiles for attachment and detachment of vanadium cations to and from the SO_3^- group of Nafion in aqueous solution at 300 K, from CPMD metadynamics using the simulation box shown on Fig. 4.

Vanadium ion	Detachment	Attachment
V^{2+}	0.37	Spontaneous
V^{3+}	0.62	Spontaneous
VO^{2+}	0.30	>0.3
VO_2^+	0.27	>0.3

activation barrier height since SS species are always diffusing away from the SO_3^- group into the bulk solution in metadynamics simulations when the accumulated energy becomes over 0.3 eV. Overall, these CPMD results reaffirm our gas-phase calculations suggesting that the most stable vanadium−Nafion complex is for V^{3+}, as indicated by the largest driving force for this ion to transform from SS to CP configuration (ΔH^f_{CP} - ΔH^f_{SS} in Table 1), zero activation barrier for adsorption and the largest barrier for desorption.

It should be pointed out that the Nafion membrane used in our study was not subjected to battery cycling, the oxidation states of vanadium were confirmed by UV−Vis measurements, while the IR spectra were collected under a constant flow of dry nitrogen. This is different from some previous experimental studies where interaction between vanadium ions and Nafion membranes were analyzed in air after VRFB charge-discharge cycling. Specifically, it was shown using UV/Vis spectroscopy [21] that the vanadyl VO^{2+} cations are the dominant species inside the Nafion membrane in the cycled Nafion membrane. Thus, the absence of V^{2+} and V^{3+} inside the Nafion observed previously after cycling in a VRFB [21] could be explained by either their oxidation in air or/and side reactions with VO_2^+ species to yield VO^{2+} during charge-discharge cycling [52].

4.4. Calculations of IR spectra, normal mode analysis and comparison with experiment

4.4.1. Nafion

The insights obtained into the mechanisms of interaction between aqueous cations and Nafion membrane allow us to analyze the influence on the IR spectrum of Nafion by metal cations. To ensure the validity of the results we obtain for IR spectra of vanadium−Nafion systems, we first compare our IR results for pure Nafion ionomer in the gas-phase with previous DFT modeling studies such as the work done by Warren et al. [32]. Our basic structural Nafion model is shown in Fig. 1 along with the reference structure used in Ref. [32]. The DFT computed frequencies and normal mode assignments (NMA) for selected number of modes are presented in Table 3, whereas the videos of the corresponding normal mode vibrations are provided in Supporting Information. Overall, our results are in full agreement with previous computational studies of pure Nafion, while small differences in NMA can be explained by the use of slightly different model structures of the Nafion ionomer.

4.4.2. Vanadium−Nafion complexes

In this section we analyze the calculated IR spectra of vanadium−Nafion systems along with the normal mode assignments and use it to explain experimentally observed spectra. All the peaks above 1800 cm^{-1} (see Fig. 2) are known to belong to OH vibrational

Table 3
Calculated frequencies (in cm^{-1}) and normal mode analysis (NMA) for Nafion model systems.

This work				Previous work (reference structure) [32]	
Visualization	B3LYP	X3LYP	NMA	B3LYP	NMA
Video-A.1	803	808	$SO_3^-{}_{vas}$, CF_{vs}, C-O-C δ	802	C-O-C_{vs}, CF_{2vs}
Video-A.5	1192	1200	$SO_3^-{}_{vas}$, CF_{vas}, C-O - C_{vs}	1186	CF_{vas}
Video-A.5	1200	1206	$SO_3^-{}_{vas}$, CF_{vas}, C-O-C_{vs}	1202	CF_{2vas}
Video-A.7	1290	1299	CF_{vs}, C-O-C ρ, C-C_{vs}	1296	C-C_{vs}
Video-A.10	1400	1406	OH bend, $SO_3^-{}_{vas}$, CF_{3vs}, CF_{2vas}	1390	$SO_3^-{}_{vas}$

Literature's computational detail: DFT with B3LYP and 6-311G + (d,p) basis set for all atoms Vibrational assignments: $_{vas}$: asymmetrical stretch, $_{vs}$: symmetrical stretch, δ: scissoring, ρ: rocking, ω: wagging, τ: twisting, var vib: various types of vibration.

Table 4
NMA for selected modes of the V^{2+}–Nafion CP complex.

V^{2+}			Nafion		
Visualization	Freq (cm^{-1})	NMA	Freq (cm^{-1})	NMA	Visualization
Video-B.1	925	$SO_3^-{}_{vs}$, var CF_2 vib, C-O-C δ			
			965	$SO_3^-{}_{vas}$, CF_{3vs}, $CF_2\omega$, C-O-C δ	Video-A.2
Video-B.2	1192	$SO_3^-{}_{vas}$, CF_{vas}, C-O-C_{vs}	1192	CF_{vas}	Video-A.5
Video-B.3	1203	$SO_3^-{}_{vas}$, CF_{vas}, C-O-C_{vs}	1206	$SO_3^-{}_{vs}$, CF_{2vas}, C-O-C_{vs}	Video-A.5
Video-B.4	1292	$SO_3^-{}_{vas}$, CF_{3vs}, CF_{2vas}, C-O-C ρ	1290	CF_{vs}, C-O-C ρ, C-C_{vs}	Video-A.7
Video-B.5	1344	CF_{vs}, C-O-C ρ, C-C_{vs}	1330	CF_{vs}, C-O-C_{vas}, C-C_{vs}	Video-A.9
			1399	OH bending, $SO_3^-{}_{vas}$, CF_{3vs}, CF_{2vas}	Video-A.10

Vibrational assignments: $_{vas}$: asymmetrical stretch, $_{vs}$: symmetrical stretch, δ: scissoring, ρ: rocking, ω: wagging, τ: twisting, var vib: various types of vibration.

modes, while the peaks centered around 1600 cm^{-1} are due to the presence of hydrogen bonds in the Nafion systems. All of these water-related vibrations for different degrees of Nafion hydration have been thoroughly investigated both theoretically and experimentally using various analytical techniques [45,46,53–59] and will not be discussed further in this work. Rather, we focus on the spectral region (500 cm^{-1} – 1350 cm^{-1}) associated with Nafion and the interactions between vanadium ions and the SO_3^- group of Nafion. Since some qualitative differences were observed experimentally between vanadium and Li^+, Na^+ ions, we also analyze these systems.

The vibrational spectum of Nafion is dense with strongly overlapping bands arising from its carbon-based backbone, which made the analysis of the Nafion skeleton complicated. With the aid of *ab initio* computations, the peaks from the overlapping region can be separated and all the contributing modes can be assigned. In this study we focus on the effects brought by aqueous cations due to their interactions with the sulfonic group of Nafion. Selected vibrational modes from the region of SO_3^- vibrations are collected in Tables 4–7 for each vanadium–Nafion CP complex and compared with the frequencies of bare Nafion.

The binding of aqueous V^{2+} cation to the SO_3^- group in a CP configuration gives rise to two extra peaks at 925 cm^{-1} and 1214 cm^{-1}, while the peak at 965 cm^{-1} of the bare Nafion disappears. It is observed that the S–O–V bond is not active in the vibrations, and the only vibrations that involve V–O bond are induced by the vibrations of S–O bond of the SO_3^- group. The peaks whose frequencies and modes are mainly affected by the presence of V^{2+} cation are summarized in Table 4.

As compared to V^{2+}, the effect of V^{3+} cation binding to the SO_3^- site of Nafion on the IR spectrum is more pronounced. This is consistent with our gas- and aqueous-phase simulations indicating that it is V^{3+} that is characterized by the strongest binding energy among all four vanadium species and barrierless kinetics of attachment to SO_3^-. It is seen from Table 5 that the S–O–V stretching mode is activated at 819 cm^{-1} with some contribution coming from the asymmetric stretch of SO_3^- ($SO_3^-{}_{vas}$). The 1330 cm^{-1} peak that was observed in protonated Nafion as a singlet is now split into a doublet of 1347 cm^{-1} and 1354 cm^{-1} frequencies with an extra contribution coming from the $SO_3^-{}_{vas}$ vibrations.

For the VO^{2+}–Nafion system, there are a few modes characterized by active S–O–V vibrations (Table 6). The 1101 cm^{-1} and 1108 cm^{-1} peaks are a doublet with a very similar set of activated vibrations. These frequencies are close to the 1115 cm^{-1} peak of bare Nafion with similar vibrational signature, and is hence the result of the 1115 cm^{-1} mode splitting induced by VO^{2+} binding. When comparing the 1295 cm^{-1} peak of VO^{2+} to the peak at 1290 cm^{-1} of Nafion, we see that the activated vibrations arise from the same bonds in both cases, however, none of the vibrational modes is the same. The S-O-V bond is directly involved and activated at three different frequencies, 908, 1134 and 1146 cm^{-1}. We also note here that VO^{2+} breaks the symmetry of the SO_3^- stretches at 981 and 1004 cm^{-1} even in the solvent share configuration (not listed in Table 6).

The formation of the VO_2^+–Nafion complex is found to influence the frequencies and contributing normal modes to the extent that although the shape of the spectrum is still similar to that of Nafion, no correlation can be made between the contributing vibrational modes of certain frequency in VO_2^+ in vanadium–Nafion complex to the area around that particular frequency in the vibrational spectroscopy of Nafion. Therefore, the shifts of the peaks in the vibrational spectum of VO_2^+ in vanadium–Nafion complex were too convoluted and the changes in the activated vibrational modes can no longer be traced from those frequencies in Nafion. The complete list of the frequencies that VO_2^+

Table 5
NMA for selected modes of the V^{3+}–Nafion CP complex.

V^{3+}			Nafion		
Visualization	Freq (cm^{-1})	NMA	Freq (cm^{-1})	NMA	Visualization
Video-C.1	819	S-O-V, H-bond, var OH vib, $SO_3^-{}_{vas}$, CF_{vs}, C-O-C_{vs}			
Video-C.2	932	var OH vib, $SO_3^-{}_{vas}$, CF_{3vs}, var CF_2 vib, C-O-C_{vs}			
			1092	CF_{vs}, C-O-C νas	Video-A.3
Video-C.3	1282	CF_{3vas}, CF_{2vs}, C-O-C_{vs}, C-Cω	1259	CF_{3vas}, CF_{2vs}, C-O-C_{vas}	Video-A.6
Video-C.4	1329	$SO_3^-{}_{vas}$, CF_{3vs}, $CF_2\omega$, C-O-C νas, C-C_{vs}	1318	CF_{vs}, C-O-C ω, C-C_{vs}	Video-A.8
			1318	CF_{vs}, C-O-C ω, C-C_{vs}	Video-A.8
Video-C.5	1347&1354	CF_{vs}, C-O-C ρ, C-C_{vs}	1330	CF_{vs}, C-O-C_{vas}, C-C_{vs}	Video-A.9
			1399	OH bending, $SO_3^-{}_{vas}$, CF_{3vs}, CF_{2vas}	Video-A.10

Vibrational assignments: $_{vas}$: asymmetrical stretch, $_{vs}$: symmetrical stretch, δ: scissoring, ρ: rocking, ω: wagging, τ: twisting, var vib: various types of vibration.

Table 6
NMA for selected modes of the VO^{2+}−Nafion CP complex.

VO^{2+}			Nafion		
Visualization	Freq (cm^{-1})	NMA	Freq (cm^{-1})	NMA	Visualization
Video-D.1	908	S-O-V, V-O stretch, OH ρ, $SO_3^-{}_{vs}$, CF_{3vs}, var CF_2 vib, C-O-Cδ			
Video-D.2	1077	V-O stretch, var OH vib, $SO_3^-{}_{vas}$, CF_{vs},C-O-C_{vas}	1092	CF_{vs},C-O-C_{vas}	Video-A.3
Video-D.3	1101	V-O strech, var OH vib, $SO_3^-{}_{vas}$, CF_{vs}, C-O-C τ			
Video-D.4	1108	V-O strech, var OH vib, $SO_3^-{}_{vas}$, CF_{vs}, C-O-C τ			
Video-D.5	1134	S-O-V, V-O stretch, OH $_{vas}$, $SO_3^-{}_{vas}$, CF_{2vs}, C-O-C_{vas}			
Video-D.6	1146	S-O-V, V-O stretch, $SO_3^-{}_{vas}$, CF_{3vas}, var CF_2 vib, C-O-C_{vas}			
Video-D.7	1186	CF_{vas}, C-O-C ω	1175	OH ρ, $SO_3^-{}_{vas}$, CF_{vas}, C-O-C ω	Video-A.4
Video-D.8	1295	CF_{vas}, C-O-C τ, C-C_{vs}	1290	CF_{vs}, C-O-Cρ, C-C_{vas}	Video-A.7
			1399	OH bending, $SO_3^-{}_{vas}$, CF_{3vs}, CF_{2vas}	Video-A.10

Vibrational assignments: $_{vas}$: asymmetrical stretch, $_{vs}$: symmetrical stretch, δ: scissoring, ρ: rocking, ω: wagging, τ: twisting, var vib: various types of vibration.

Table 7
NMA for selected modes of the VO_2^+−Nafion CP complex.

Visualization	Freq (cm^{-1})	NMA
Video-E.1	774	S-O-V, V-O_{vs}, OH δ, $SO_3^-{}_{vs}$, CF_{3vs}, CF_2 ρ, C-O-C_{vs}
Video-E.2	805	S-O-V, OH δ, $SO_3^-{}_{vs}$, CF_{3vs},CF_3 ω C-O-C_{vs}
Video-E.3	812	S-O-V, V-O_{vs}, OH δ, $SO_3^-{}_{vs}$, CF_{3vas},CF_2 ω, C-O-C_{vs}
Video-E.4	923	S-O-V, V-O_{vs}, OH ω, $SO_3^-{}_{vs}$, CF_{3vs}, var CF_2 vib, C-O-C δ
Video-E.5	1003	S-O-V, V-O_{vs}, $SO_3^-{}_{vs}$, CF_{3vs}, $CF_2\omega$, C-O-C δ
Video-E.6	1052	V-O_{vas}, OH δ, $SO_3^-{}_{vas}$, CF_2 ω, C-O-C δ
Video-E.7	1092	V-O_{vs}, OH ω $SO_3^-{}_{vs}$, var CF_2 vib,C-O-C δ
Video-E.8	1103	V-O_{vs}, OH ω, $SO_3^-{}_{vas}$, CF_{3vas}, CF_{2vs}, C-O-C_{vas}
Video-E.9	1116	S-O-V, V-O_{vs}, OH ω, $SO_3^-{}_{vas}$, CF_{vs}, C-O-C τ
Video-E.10	1124	S-O-V, V-O_{vs}, $SO_3^-{}_{vas}$, CF_{3vs}, var CF_2 vib, C-O-C_{vas}
Video-E.11	1160	V-O_{vs}, $SO_3^-{}_{vs}$, CF_{3vas}, CF_2 ρ, C-O-C τ, C-C ρ

Vibrational assignments: $_{vas}$: asymmetrical stretch, $_{vs}$: symmetrical stretch, δ: scissoring, ρ: rocking, ω: wagging, τ: twisting, var vib: various types of vibration.

vibrations in vanadium - Nafion complex is given in Table 7.

In the same way as we compared the effect of the exchange-correlation functional on the IR spectrum of Nafion and the energetics of formation for vanadium−Nafion complexes, we also analyze the results obtained by two different functionals B3LYP and X3LYP on the example of V^{2+}−Nafion system. The frequencies of all computed normal modes are in good agreement when using the B3LYP or X3LYP functionals (within 10 cm-1), although X3LYP tends to register systematically slightly higher frequencies for a specific computed peak. This systematic blue shift by X3LYP functional can be attributed to a little more accurate description of the heats of formation in X3LYP, in agreement with the work done by Webber et al. [50].

4.4.3. Comparison with Li^+ and Na^+ cases

From the experimental IR shown in Fig. 2, it is observed that the main difference between the IR spectra of V^{z+}−Nafion and Li^+/Na^+−Nafion systems is observed in the 950 cm^{-1} - 1000 cm^{-1} region (shown in Fig. 6) where V^{z+}−Nafion complexes have two pronounced peaks while Li^+/Na^+−Nafion complexes have only one band with the second band being significantly diminished. Based on the symmetry argument, splitting of the doubly degenerate symmetric SO_3^- stretching mode with C_{3v} symmetry is expected for both mono- and bi-dentate cation−Nafion structures as the local symmetry of the SO_3^- group is reduced to the C_s symmetry upon coordinating to the cations. According to our gas-phase and solution DFT simulations, mono-dentate CP are energetically more favorable structures than SS for all four vanadium ions. DFT-based normal mode analysis for vanadium CP complexes indicates that the symmetry is indeed lowered resulting in the asymmetric SO_3^- stretching as shown by the arrows in Fig. 6 and the corresponding eigenvector animations on the example of the V^{3+}−Nafion CP structure (see Table 8).

In the case of Li^+/Na^+−Nafion, however, we find that CP and SS configurations are almost equally stable based on the enthalpy of formation and fast transformation between CP and SS configurations detected in CPMD simulations at 300 K. This might reflect the competition between Li^+/Na^+ and SO_3^- electrostatic interactions and the tendency for Li^+ and Na^+ to be solvated. Moreover, even when analyzing eigenvector animations for the CP configuration of both Li^+- and Na^+−Nafion, which should result in the lifting of the C_{3v} symmetry, we still observe a symmetric SO_3^- stretch (see Fig. 6). This can be attributed to a relatively weak interaction between aqueous Li^+- and Na^+ species and the SO_3^- group of Nafion rendering equal probability of CP and SS structures. This interaction even for CP configuration is thus not strong enough to break the C_{3v} symmetry of SO_3^- which may explain the absence of the second peak in the experimentally measured IR spectra for Li and Na systems.

5. Conclusions

Interactions between aqueous vanadium, Li^+ and Na^+ species and Nafion membrane were investigated by a combination of IR spectroscopy, static DFT and Car-Parrinello molecular dynamics (CPMD) simulations. Measured IR spectra for the non-cycled membrane indicated that the main difference across various systems is observed in the 950 cm^{-1} - 1000 cm^{-1} spectral region which corresponds to vibrations of SO_3^- head group of Nafion and thus suggests different interaction mechanisms between SO_3^- and the cationic species. It was found that all four vanadium cations (V^{2+}, V^{3+} VO^{2+}, and VO_2^+) thermodynamically tend to bind to the SO_3^- head group of Nafion via the contact pair mechanism as the mono-dentate complex rather than via a solvent share mechanism. Stability of these vanadium−Nafion complexes in aqueous solution at 300 K was further confirmed by CPMD simulations.

To gain insights into the kinetics of cation-Nafion interactions, CPMD-based metadynamics simulations of aqueous solutions at room temperature were performed. The computed free-energy profiles suggest that V^{2+} and V^{3+} should spontaneously attach to SO_3^-, while VO^{2+} and VO_2^+ are both characterized by relatively high barriers (>0.3 eV) for attachment. Once attached, all species exhibit sizable activation barriers for detachment from the SO_3^- sites. Combined with previous

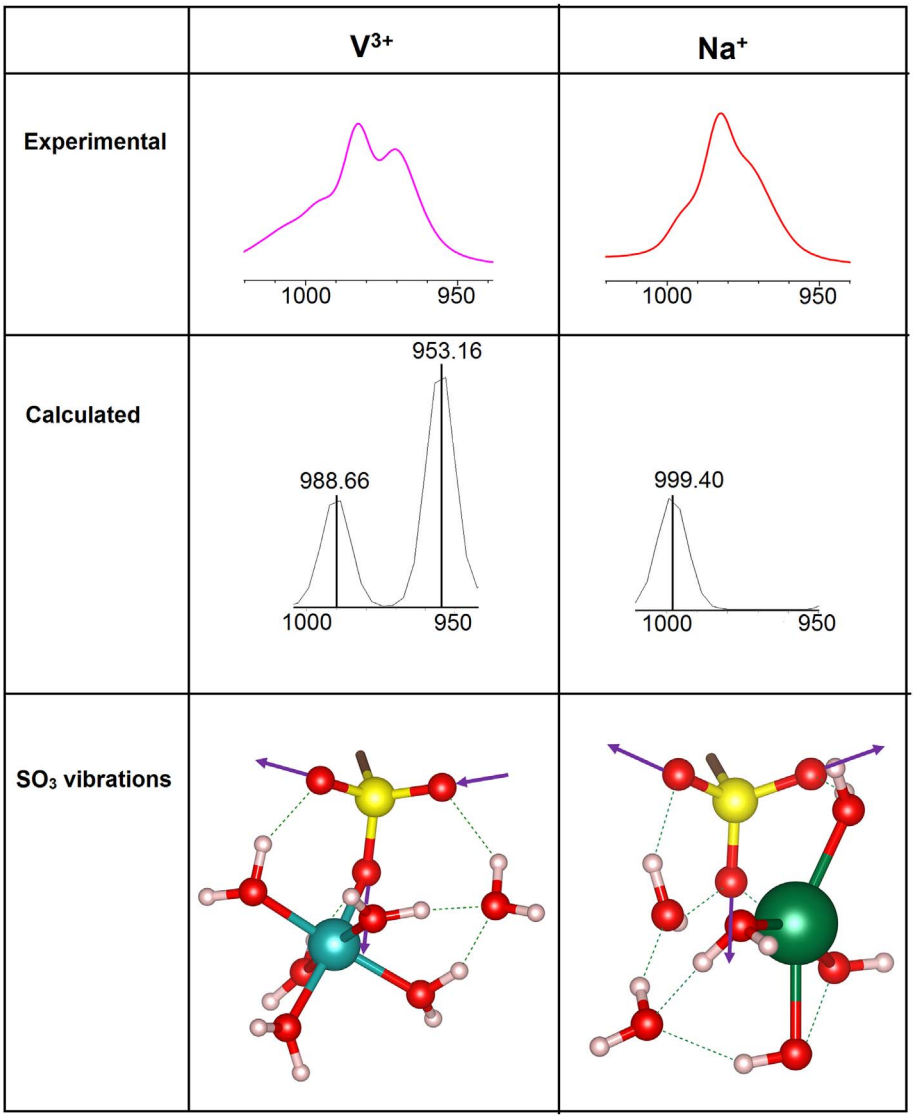

Fig. 6. Comparison between experimental infrared peaks and calculated peaks that registered in the 950 cm^{-1}–1000 cm^{-1} range and normal modes vibrations of SO_3^- group of V^{3+} and Na^+. Color representation: as in Table 2. (For interpretation of the references to colour in this figure legend, the reader is referred to the web version of this article.)

Table 8
Comparison of the peaks between V^{3+} and Na^+ within 950 cm^{-1}–1000 cm^{-1} frequency range.

Contact Pair					
V^{3+}			Na^+		
Visualization	Freq (cm^{-1})	NMA	Freq (cm^{-1})	NMA	Visualization
Video-F.1	954	S-O-V, $SO_3^-{}_{vas}$, CF_{3vs}, CF_2 var, C-O-C δ, C-C_{vs}			
Video-F.2	990	S-O-V, $SO_3^-{}_{vas}$, CF_{3vs}, S-O-V, CF_2 var, C-O-C τ, C-C ρ	987	S-O-Na, $SO_3^-{}_{vs}$, CF_{3vs},	Video-F.3
Solvent Share					
	Freq (cm^{-1})	NMA	Freq (cm^{-1})	NMA	
Video-F.4	954	$SO_3^-{}_{vas}$, CF_3 var, CF_2 var, C-O-C δ, C-C ω			
Video-F.5	998	$SO_3^-{}_{vas}$, CF_{3vs}, CF_2 var, C-O-C τ, C-C_{vas}	987	$SO_3^-{}_{vs}$, CF_{3vs}, CF_{2vs},	Video-F.6

Vibrational assignments: $_{vas}$: asymmetrical stretch, $_{vs}$: symmetrical stretch, δ: scissoring, ρ: rocking, ω: wagging, τ: twisting, var vib: various types of vibration.

experimental observations for the cycled Nafion membrane in a VRFB where primarily VO^{2+} was detected inside the membrane, these results suggest that V^{2+} and V^{3+} species are consumed by either their oxidation in air or/and side reactions with VO_2^+ species to yield VO^{2+} during charge-discharge cycling.

Acknowledgements

This work was supported by the Nebraska Center for Energy Sciences Research at the University of Nebraska-Lincoln and the startup package provided by the University of Nebraska-Lincoln. This research used resources of the National Energy Research Scientific Computing Center, a DOE Office of Science User Facility supported by the Office of Science of the U.S. Department of Energy under Contract No. DE-AC02-05CH11231 and the Extreme Science and Engineering Discovery Environment (XSEDE) supported by the National Science Foundation. Experimental infrastructure support was provided by the Pennsylvania State University Materials Research Institute and the Penn State Institutes of Energy & the Environment. M. A. H. acknowledges the Corning Foundation and the Corning Faculty Fellowship in Materials Science and Engineering for support.

Appendix A. Supplementary data

Supplementary data related to this article can be found at http://dx.doi.org/10.1016/j.jpowsour.2017.10.050.

References

[1] C.P. de Leon, A. Frias-Ferrer, J. Gonzalez-Garcia, D.A. Szanto, F.C. Walsh, Redox flow cells for energy conversion, J. Power Sources 160 (1) (2006) 716–732.
[2] G.L. Soloveichik, Flow batteries: current status and trends, Chem. Rev. 115 (20) (2015) 11533–11558.
[3] F. Pan, Q. Wang, Redox species of redox flow batteries: a review, Molecules 20 (11) (2015) 20499–20517.
[4] E. Sum, M. Rychcik, M. Skyllas-Kazacos, Investigation of the V(V)/V(IV) system for use in the positive half-cell of a redox battery, J. Power Sources 16 (2) (1985) 85–95.
[5] Y. Shao, X. Wang, M. Engelhard, C. Wang, S. Dai, J. Liu, Z. Yang, Y. Lin, Nitrogen-doped mesoporous carbon for energy storage in vanadium redox flow batteries, J. Power Sources 195 (13, SI) (2010) 4375–4379.
[6] M. Vijayakumar, S.D. Burton, C. Huang, L. Li, Z. Yang, G.L. Graff, J. Liu, J. Hu, M. Skyllas-Kazacos, Nuclear magnetic resonance studies on V(IV) electrolyte solutions for vanadium redox flow battery, J. Power Sources 195 (22, SI) (2010) 7709–7717.
[7] M. Vijayakumar, L. Li, G. Graff, J. Liu, H. Zhang, Z. Yang, J.Z. Hu, Towards understanding the poor thermal stability of V^{5+} electrolyte solution in vanadium redox flow batteries, J. Power Sources 196 (7, SI) (2011) 3669–3672.
[8] M. Skyllas-Kazacos, M. Chakrabarti, S. Hajimolana, F. Mjalli, M. Saleem, Progress in flow battery research and development, J. Electrochem. Soc. 158 (8) (2011) R55–R79.
[9] K.J. Kim, M.-S. Park, Y.-J. Kim, J.H. Kim, S.X. Dou, M. Skyllas-Kazacos, A technology review of electrodes and reaction mechanisms in vanadium redox flow batteries, J. Mater. Chem. A 3 (33) (2015) 16913–16933.
[10] Z. Jiang, K. Klyukin, V. Alexandrov, Structure, hydrolysis, and diffusion of aqueous vanadium ions from Car-Parrinello molecular dynamics, J. Chem. Phys. 145 (11) (2016) 114303–114311.
[11] Z. Jiang, K. Klyukin, V. Alexandrov, First-principles study of adsorption–desorption kinetics of aqueous V^{2+}/V^{3+} redox species on graphite in a vanadium redox flow battery, Phys. Chem. Chem. Phys. 19 (23) (2017) 14897–14901.
[12] X. Li, H. Zhang, Z. Mai, H. Zhang, I. Vankelecom, Ion exchange membranes for vanadium redox flow battery (VRB) applications, Energy & Environ. Sci. 4 (4) (2011) 1147–1160.
[13] B. Schwenzer, J. Zhang, S. Kim, L. Li, J. Liu, Z. Yang, Membrane development for vanadium redox flow batteries, ChemSusChem 4 (10) (2011) 1388–1406.
[14] P. Swaminathan, P. Disley, H. Assender, Surface modification of ion exchange membrane using amines, J. Membr. Sci. 234 (1) (2004) 131–137.
[15] H. Prifti, A. Parasuraman, S. Winardi, T.M. Lim, M. Skyllas-Kazacos, Membranes for redox flow battery applications, Membranes 2 (2) (2012) 275–306.
[16] DuPont, Nafion, PFSA Membranes N-112, NE-1135, N-115, N-117, NE-1110 Perfluorosulfonic Acid Polymer, product information: NAE101, (Nov 2002).
[17] K.-D. Kreuer, Proton conductivity: materials and applications, Chem. Mater. 8 (3) (1996) 610–641.
[18] A. Kusoglu, A.Z. Weber, New insights into perfluorinated sulfonic-acid ionomers, Chem. Rev. 117 (3) (2017) 987–1104.
[19] A.J.A. Aquino, D. Tunega, Ab initio molecular dynamics simulations on the hydrated structures of Nafion models, J. Phys. Chem. C 121 (21) (2017) 11215–11225.
[20] M. Vijayakumar, N. Govind, B. Li, X. Wei, Z. Nie, S. Thevuthasan, V. Sprenkle, W. Wang, Aqua-vanadyl ion interaction with Nafion® membranes, Front. Energy Res. 3 (2015) 10.
[21] M. Vijayakumar, M. Bhuvaneswari, P. Nachimuthu, B. Schwenzer, S. Kim, Z. Yang, J. Liu, G.L. Graff, S. Thevuthasan, J. Hu, Spectroscopic investigations of the fouling process on nafion membranes in vanadium redox flow batteries, J. Membr. Sci. 366 (1) (2011) 325–334.
[22] F. Sepehr, S.J. Paddison, Effect of sulfuric and triflic acids on the hydration of vanadium cations: an ab initio study, J. Phys. Chem. A 119 (22) (2015) 5749–5761.
[23] S. Lowry, K. Mauritz, An investigation of ionic hydration effects in perfluorosulfonate ionomers by Fourier transform infrared spectroscopy, J. Am. Chem. Soc. 102 (14) (1980) 4665–4667.
[24] R.M. Blanchard, R.G. Nuzzo, An infrared study of the effects of hydration on cation-loaded Nafion thin films, J. Polym. Sci. part B Polym. Phys. 38 (11) (2000) 1512–1520.
[25] J. Doan, N.E. Navarro, D. Kumari, K. Anderson, E. Kingston, C. Johnson, A. Vong, N. Dimakis, E.S. Smotkin, Symmetry-based IR group modes as dynamic probes of Nafion ion exchange site structure, Polymer 73 (2015) 34–41.
[26] N. Loupe, N. Nasirova, J. Doan, D. Valdez, M. Furlani, N. Dimakis, E. S. Smotkin, DFT-experimental IR spectroscopy of lithiated single ion conducting perfluorinated sulfonated ionomers: ion induced polarization band broadening, J. Electroanal. Chem..
[27] I. Kendrick, A. Yakaboski, E. Kingston, J. Doan, N. Dimakis, E.S. Smotkin, Theoretical and experimental infrared spectra of hydrated and dehydrated Nafion, J. Polym. Sci. Part B Polym. Phys. 51 (18) (2013) 1329–1334.
[28] W.W. Huang, R. Frech, R.A. Wheeler, Molecular-structures and normal vibrations of $CF_3SO_3^-$ and its lithium ion-pairs and aggregates, J. Phys. Chem. 98 (1) (1994) 100–110.
[29] A.D. Becke, Density-functional thermochemistry. iii. The role of exact exchange, J. Chem. Phys. 98 (7) (1993) 5648–5652.
[30] M. Valiev, E.J. Bylaska, N. Govind, K. Kowalski, T.P. Straatsma, H.J. Van Dam, D. Wang, J. Nieplocha, E. Apra, T.L. Windus, et al., NWChem: a comprehensive and scalable open-source solution for large scale molecular simulations, Comput. Phys. Commun. 181 (9) (2010) 1477–1489.
[31] X. Xu, Q. Zhang, R.P. Muller, W.A. Goddard III, An extended hybrid density functional (X3LYP) with improved descriptions of nonbond interactions and thermodynamic properties of molecular systems, J. Chem. Phys. 122 (1) (2005) 014105.
[32] D.S. Warren, A.J. McQuillan, Infrared spectroscopic and DFT vibrational mode study of perfluoro (2-ethoxyethane) sulfonic acid (pes), a model Nafion side-chain molecule, J. Phys. Chem. B 112 (34) (2008) 10535–10543.
[33] R. Car, M. Parrinello, Unified approach for molecular dynamics and density-functional theory, Phys. Rev. Lett. 55 (22) (1985) 2471.
[34] J.P. Perdew, K. Burke, M. Ernzerhof, Generalized gradient approximation made simple, Phys. Rev. Lett. 77 (18) (1996) 3865.
[35] N. Troullier, J.L. Martins, Efficient pseudopotentials for plane-wave calculations, Phys. Rev. B 43 (3) (1991) 1993.
[36] D. Hamann, M. Schlüter, C. Chiang, Norm-conserving pseudopotentials, Phys. Rev. Lett. 43 (20) (1979) 1494.
[37] D. Hamann, Generalized norm-conserving pseudopotentials, Phys. Rev. B 40 (5) (1989) 2980.
[38] S. Nosé, A molecular dynamics method for simulations in the canonical ensemble, Mol. Phys. 52 (2) (1984) 255–268.
[39] W.G. Hoover, Canonical dynamics: equilibrium phase-space distributions, Phys. Rev. A 31 (3) (1985) 1695.
[40] E. Cauët, S. Bogatko, J.H. Weare, J.L. Fulton, G.K. Schenter, E.J. Bylaska, Structure and dynamics of the hydration shells of the Zn^{2+} ion from ab initio molecular dynamics and combined ab initio and classical molecular dynamics simulations, J. Chem. Phys. 132 (19) (2010) 194502.
[41] C. Micheletti, A. Laio, M. Parrinello, Reconstructing the density of states by history-dependent metadynamics, Phys. Rev. Lett. 92 (17) (2004) 170601.
[42] A. Laio, F.L. Gervasio, Metadynamics: a method to simulate rare events and reconstruct the free energy in biophysics, chemistry and material science, Rep. Prog. Phys. 71 (12) (2008) 126601.
[43] Chemcraft, http://chemcraftprog.com.
[44] K. Singh Boparai, R. Singh, H. Singh, Experimental investigations for development of Nylon6-Al-Al_2O_3 alternative FDM filament, Rapid Prototyp. J. 22 (2) (2016) 217–224.
[45] M. Falk, An infrared study of water in perfluorosulfonate (Nafion) membranes, Can. J. Chem. 58 (14) (1980) 1495–1501.
[46] A. Gruger, A. Régis, T. Schmatko, P. Colomban, Nanostructure of Nafion® membranes at different states of hydration: an IR and Raman study, Vib. Spectrosc. 26 (2) (2001) 215–225.
[47] N. Ramaswamy, N. Hakim, S. Mukerjee, Degradation mechanism study of perfluorinated proton exchange membrane under fuel cell operating conditions, Electrochim. Acta 53 (8) (2008) 3279–3295.
[48] R. Buzzoni, S. Bordiga, G. Ricchiardi, G. Spoto, A. Zecchina, Interaction of H_2O, CH_3OH, $(CH_3)_2O$, CH_3CN, and pyridine with the superacid perfluorosulfonic membrane Nafion: an IR and Raman study, J. Phys. Chem. 99 (31) (1995) 11937–11951.
[49] S.P. Gejji, K. Hermansson, J. Lindgren, Ab initio vibrational frequencies of the triflate ion $CF_3SO_3^-$, J. Phys. Chem. 97 (15) (1993) 3712–3715.
[50] M. Webber, N. Dimakis, D. Kumari, M. Fuccillo, E.S. Smotkin, Mechanically coupled internal coordinates of ionomer vibrational modes, Macromolecules 43 (13) (2010) 5500–5502.
[51] F. Sepehr, S.J. Paddison, The solvation structure and thermodynamics of aqueous

vanadium cations, Chem. Phys. Lett. 585 (2013) 53–58.
[52] E. Agar, K. Knehr, D. Chen, M. Hickner, E. Kumbur, Species transport mechanisms governing capacity loss in vanadium flow batteries: comparing Nafion® and sulfonated radel membranes, Electrochim. Acta 98 (2013) 66–74.
[53] R. Basnayake, G.R. Peterson, D.J. Casadonte, C. Korzeniewski, Hydration and interfacial water in Nafion membrane probed by transmission infrared spectroscopy, J. Phys. Chem. B 110 (47) (2006) 23938–23943.
[54] R. Basnayake, W. Wever, C. Korzeniewski, Hydration of freestanding Nafion membrane in proton and sodium ion exchanged forms probed by infrared spectroscopy, Electrochim. Acta 53 (3) (2007) 1259–1264.
[55] G.S. Hwang, M. Kaviany, J.T. Gostick, B. Kientiz, A.Z. Weber, M.H. Kim, Role of water states on water uptake and proton transport in Nafion using molecular simulations and bimodal network, Polymer 52 (12) (2011) 2584–2593.
[56] R. Iwamoto, K. Oguro, M. Sato, Y. Iseki, Water in perfluorinated sulfonic acid Nafion membranes, J. Phys. Chem. B 106 (28) (2002) 6973–6979.
[57] M. Laporta, M. Pegoraro, L. Zanderighi, Perfluorosulfonated membrane (Nafion): FTIR study of the state of water with increasing humidity, Phys. Chem. Chem. Phys. 1 (19) (1999) 4619–4628.
[58] M. Ludvigsson, J. Lindgren, J. Tegenfeldt, FTIR study of water in cast Nafion films, Electrochim. Acta 45 (14) (2000) 2267–2271.
[59] C.-E. Tsai, B.-J. Hwang, Intermolecular interactions between methanol/water molecules and Nafion membrane: an infrared spectroscopy study, Fuel *Cells* 7 (5) (2007) 408–416.